High-precision measurements of the co-polar correlation coefficient: non-Gaussian errors and retrieval of the dispersion parameter μ in rainfall

Article

Published Version

High-Precision Measurements of the Copolar Correlation Coefficient: Non-Gaussian Errors and Retrieval of the Dispersion Parameter μ in Rainfall

W. J. KEAT, C. D. WESTBROOK, AND A. J. ILLINGWORTH

Department of Meteorology, University of Reading, Reading, United Kingdom

(Manuscript received 28 September 2015, in final form 22 March 2016)

ABSTRACT

The copolar correlation coefficient ρ_{hv} has many applications, including hydrometeor classification, ground clutter and melting-layer identification, interpretation of ice microphysics, and the retrieval of raindrop size distributions (DSDs). However, the quantitative error estimates that are necessary if these applications are to be fully exploited are currently lacking. Previous error estimates of ρ_{hv} rely on knowledge of the unknown "true" ρ_{hv} and implicitly assume a Gaussian probability distribution function of ρ_{hv} samples. Frequency distributions of ρ_{hv} estimates are in fact shown to be highly negatively skewed. A new variable, $L = \log_{10}(1 - \rho_{hv})$, is defined that does have Gaussian error statistics and a standard deviation depending only on the number of independent radar pulses. This is verified using observations of spherical drizzle drops, allowing, for the first time, the construction of rigorous confidence intervals in estimates of ρ_{hv}. In addition, the manner in which the imperfect collocation of the horizontal and vertical polarization sample volumes may be accounted for is demonstrated. The possibility of using L to estimate the dispersion parameter μ in the gamma drop size distribution is investigated. Including drop oscillations is found to be essential for this application; otherwise, there could be biases in retrieved μ of up to approximately 8. Preliminary results in rainfall are presented. In a convective rain case study, the estimates presented herein show μ to be substantially larger than 0 (an exponential DSD). In this particular rain event, rain rate would be overestimated by up to 50% if a simple exponential DSD is assumed.

1. Introduction

The copolar correlation coefficient ρ_{hv} between horizontal (H) and vertical (V) polarization radar signals is a measure of the variety of hydrometeor shapes in a pulse volume. It is therefore useful for applications such as identifying the melting layer (Caylor and Illingworth 1989; Brandes and Ikeda 2004; Tabary et al. 2006; Giangrande et al. 2008), ground clutter (e.g., Tang et al. 2014), rain–hail mixtures (Balakrishnan and Zrnić 1990) and interpreting polarimetric signatures in ice (e.g., Andrić et al. 2013), and potentially the retrieval of the drop size distribution (DSD). The standard deviations of differential reflectivity Z_{DR} and differential phase shift ϕ_{dp} are both functions of ρ_{hv} (Bringi and Chandrasekar 2001). Therefore, ρ_{hv} dictates both the quality of dual-polarization measurements and their weighting in hydrometeor classification schemes (Park et al. 2009). In rainfall, ρ_{hv} is typically 0.98–1. Giangrande et al. (2008) use data where $\rho_{hv} < 0.97$ to identify the melting layer. For hail, ρ_{hv} can be much lower because of Mie scattering. At present, quantitative use of ρ_{hv} is hampered by a lack of rigorous confidence intervals accompanying the ρ_{hv} estimates. Error estimates are available by adopting an empirical approach (Illingworth and Caylor 1991) or a linear perturbation technique (Liu et al. 1994; Torlaschi and Gingras 2003), both of which implicitly assume a Gaussian probability distribution for the ρ_{hv} samples. We will show that the distribution of ρ_{hv} samples is in fact non-Gaussian and highly negatively skewed.

Natural raindrop size distributions can be described by a gamma distribution (Ulbrich 1983):

$$N(D) = N_0 D^{\mu} \exp\left[-\frac{(3.67 + \mu)}{D_0} D\right], \qquad (1)$$

where D is the equivalent spherical drop diameter, N_0 is the intercept parameter, D_0 is the median volume drop diameter, and μ is the dispersion parameter (a measure

Corresponding author address: W. J. Keat, Dept. of Meteorology, University of Reading, Earley Gate, P.O. Box 243, Reading RG6 6BB, United Kingdom.
E-mail: w.j.keat@pgr.reading.ac.uk

DOI: 10.1175/JAMC-D-15-0272.1

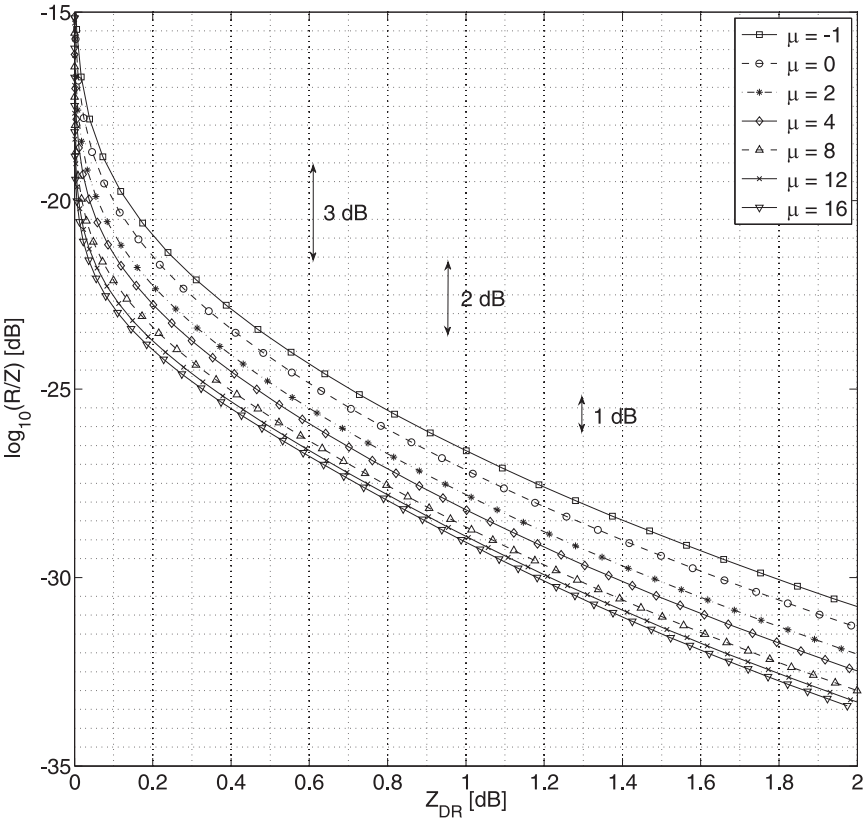

FIG. 1. Rain rate (dB, referenced to 1 mm h^{-1}) per unit radar reflectivity as a function of Z_{DR} computed using Gans theory for gamma distributions of $\mu = -1, 0, 2, 4, 8, 12$, and 16. The rain rate can vary by as much as 2.5 dB for a given pair of Z and Z_{DR} observations as a result of drop spectrum shape variability.

of the drop size spectrum shape). If $\mu = 0$, by exploiting the relationship between drop diameter and drop axis ratio, D_0 can be estimated using Z_{DR} (Seliga and Bringi 1976). Higher μ corresponds to more monodisperse drop size distributions. Since ρ_{hv} is sensitive to variations in drop shape, it can in principle be used to estimate μ (Jameson 1987), knowledge of which could improve dual-polarization and dual-frequency (e.g., the Global Precipitation Measurement satellite) rain-rate estimates. Figure 1 shows rain rate R per unit radar reflectivity Z as a function of Z_{DR} for simulated gamma distributions with $\mu = -1$, 0, 2, 4, 8, 12, and 16. The rain rate is sensitive to variability in the shape of the drop size spectrum; uncertainty in μ alone could introduce an error in the retrieved rain rate of up to 2.5 dB (almost a factor of 2) for a given pair of Z and Z_{DR} observations.

It is difficult to obtain reliable estimates of μ from observations. Disdrometers suffer from undersampling of large drops, which cause μ values that are derived from the third, fourth, and sixth moments of the drop size distribution to be biased high (Johnson et al. 2014). Furthermore, disdrometers also undercount the number of drops < 0.5 mm (Tokay et al. 2001), which can also introduce a bias in estimates of μ. Estimating DSD parameters using radar is therefore preferable, because of the very large number of drops being sampled. Wilson et al. (1997) made radar observations dwelling in rain at elevation angles above 20° and reported that the difference in the mean Doppler velocity at H and V polarizations provides an estimate of μ, which were in the range of 1 to 11, and, once Z_{DR} exceeded 0.5 dB, all the values were above 4. Doppler spectra of rain at vertical incidence with multiple wavelength radars, including wind profiler frequencies that respond to the clear-air motion, have been utilized to estimate μ (Williams 2002; Schafer et al. 2002). These experiments find μ ranges between 0 and 18, but is typically between 0 and 6. Unal (2015) fits the observed Doppler spectra to theoretical drop spectra at S band and retrieves μ in the range from -1 to 5. The disadvantage of these techniques is that they use high-elevation angles; for operational monitoring of surface rainfall, measurements at

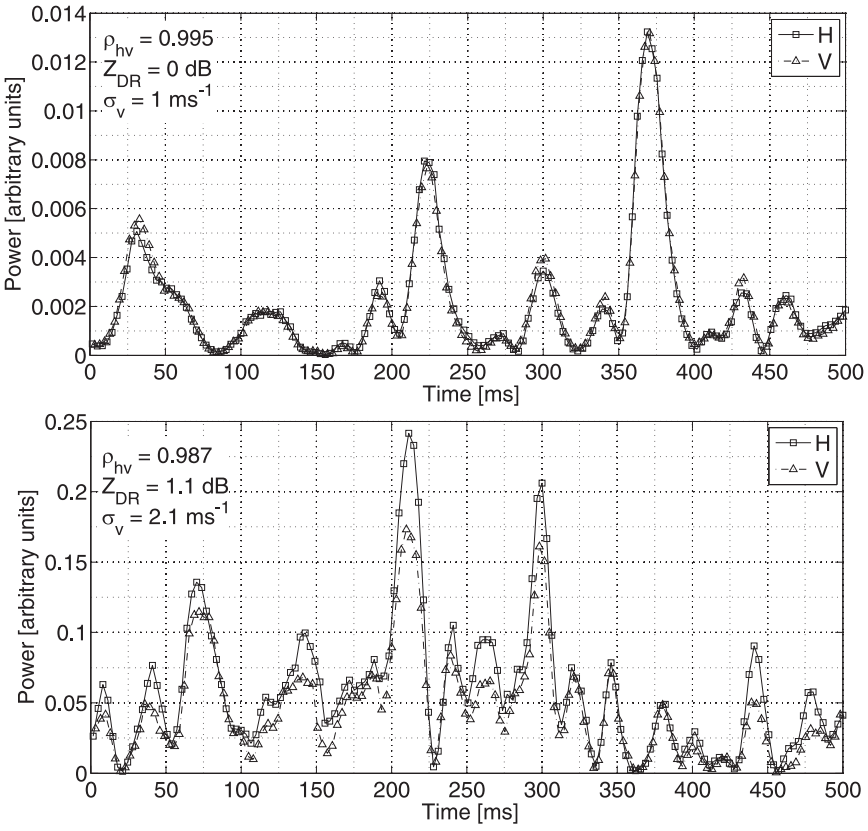

FIG. 2. Example time series (0.5 s) for single 75-m gates from 1.5°-elevation dwells in (a) drizzle (Z_{DR} = 0 dB) at 1203 UTC 6 Feb 2014 and (b) heavier rainfall (Z_{DR} = 1.1 dB) at 1706 UTC 31 Jan 2014. For both examples, SNR > 40 dB. For drizzle, the *H* and *V* echo time series vary in unison as the drops are all spherical. In heavier rainfall, the broader axis ratio distribution causes the *H* and *V* time series to be less correlated. The rate of fluctuation of the signals is determined by the Doppler spectral width.

low-elevation angles are preferable. This motivates the use of ρ_{hv} to derive μ in rainfall. Illingworth and Caylor (1991) and Thurai et al. (2008) inferred μ from the decrease in ρ_{hv} as Z_{DR} increases. The difficulty here is that any mismatches in the *H* and *V* beams will introduce an uncorrelated noise component, so that even for perfectly spherical drizzle droplets, where the true ρ_{hv} is unity, the radar will always detect a value less than one (we will call this maximum obtainable level of ρ_{hv} "f_{hv}^{max}"; see section 5). From measurements in rain at short range, Illingworth and Caylor (1991) inferred μ values, which if corrected with an estimate of f_{hv}^{max} were in the range 0–2, but even for long dwells the estimated errors in μ were quite large. Thurai et al. (2008) analyzed ρ_{hv} measurements from an operational radar and obtained estimates of μ in the range of 1–3; however, their approach relies on empirically derived relationships between ρ_{hv} and DSD widths from two-dimensional video disdrometer (2DVD) measurements. Furthermore, the technique is only valid for intense rain $Z_{DR} \geq 2$ dB and $\rho_{hv} < 0.98$).

The aim of this paper is to define a new variable, $L = -\log_{10}(1 - \rho_{hv})$, that has Gaussian error statistics with a width predictable from the number of independent radar pulses. This can be readily estimated by using the observed Doppler spectral width σ_v. We will then present measurements of L in rainfall as a function of Z_{DR}, and retrieve estimates of μ by comparing these with predicted L and Z_{DR} for various three-parameter gamma distributions. The possibility of using this technique to retrieve μ using operational radars is then discussed.

2. The copolar correlation coefficient (ρ_{hv})

The quantity ρ_{hv} is defined as (Doviak and Zrnić 2006)

$$\rho_{hv} = \frac{\langle S_{VV} S_{HH}^{*} \rangle}{\sqrt{\langle |S_{HH}|^2 \rangle \langle |S_{VV}|^2 \rangle}}, \tag{2}$$

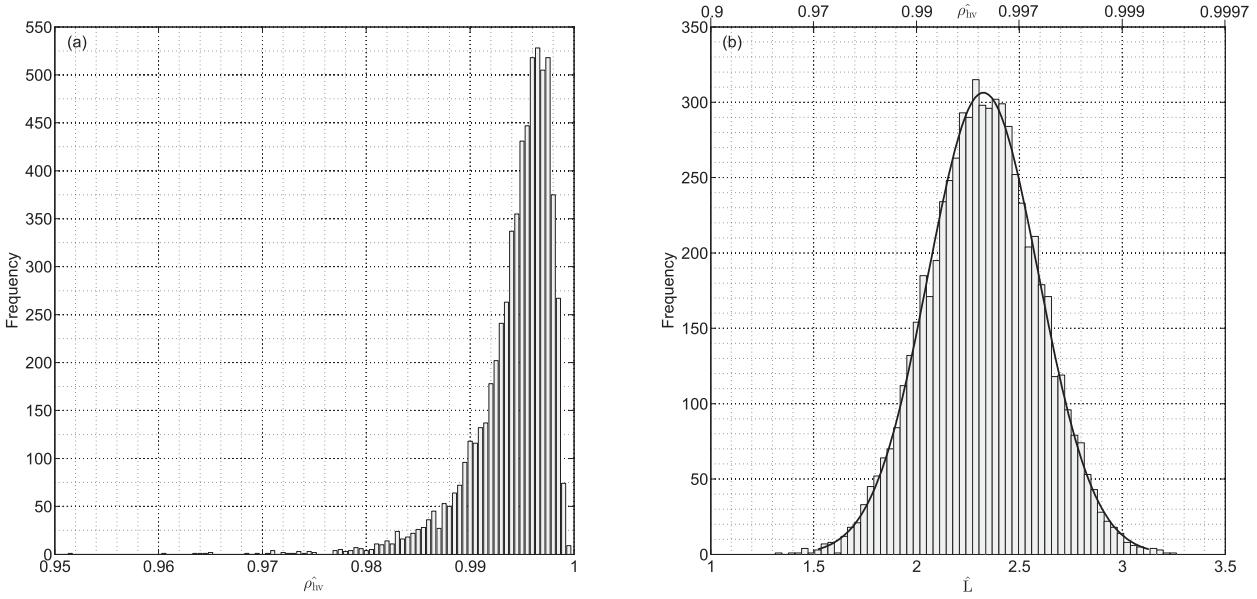

FIG. 3. The frequency distribution of (a) $\hat{\rho}_{hv}$ calculated from a total of 1159 time series (0.21 s; 75-m gates) in drizzle ($Z_{DR} < 0.1$ dB) and of (b) $\hat{L} = -\log_{10}(1 - \hat{\rho}_{hv})$. The data were collected at 1203 UTC 6 Feb 2014 during a 1.5°-elevation dwell and have very high SNR (>40 dB). The σ_v values for these data range between 0.9 and 1.3 m s^{-1}. Overplotted on $\hat{L}$ is a Gaussian curve with the same mean and standard deviation as in the measured distribution.

where $\langle S_{HH} \rangle$ and $\langle S_{VV} \rangle$ are the copolar elements of the backscattering matrix averaged over an ensemble of scatterers for the H and V polarizations, respectively, and the asterisk indicates the complex conjugate. It can be estimated by correlating successive power or complex (I and Q) measurements. Examples of power time series in drizzle and heavier rainfall from the 3-GHz Chilbolton Advanced Meteorological Radar (CAMRa) are shown in Figs. 2a and 2b, respectively. The radar is a coherent-on-receive magnetron system, transmitting and receiving alternate H- and V-polarized pulses with a pulse repetition frequency (PRF) of 610 Hz. A cubic polynomial interpolation is used to estimate the H power at the V pulse timing and the V power at the H pulse timing. Its narrow one-way half-power beamwidth (0.28°) makes it capable of very high-resolution measurements. The full capabilities of this radar are discussed in Goddard et al. (1994). The observed fluctuating signals in Fig. 2 are caused by the superposition of the backscattered waves from each drop in the sample volume; the rate of fluctuation is determined by the Doppler spectral width. For drizzle, since the drops are spherical, $Z_{DR} = 0$ dB, and the H and V signals are almost perfectly correlated: $\rho_{hv} = 0.995$. For heavier rainfall, a systematically lower V power is measured ($Z_{DR} = 1.1$ dB), and the signals are visibly less correlated ($\rho_{hv} = 0.987$), as a result of the broader axis ratio distributions in the sample volume.

These estimates of ρ_{hv} are derived from a finite number of reshufflings, and therefore there is some uncertainty in them. In what follows, we quantify this uncertainty.

3. Theoretical measurement error in estimated correlation of time series

Figure 3a shows the distribution of estimates of the correlation coefficient, $\hat{\rho}_{hv}$ (calculated from a finite length time series), as distinct from the true copolar correlation coefficient, $\overline{\rho}_{hv}$ (which would be measured for a time series of infinite length). The data were collected during a 1.5°-elevation dwell in drizzle ($Z_{DR} < 0.1$ dB), with very high signal-to-noise ratio (SNR; > 40 dB) on 6 February 2014. Each $\hat{\rho}_{hv}$ is calculated from 64 H and V pulse pairs (0.21-s dwell) from 75-m range gates with $\sigma_v = 1.1 \pm 0.1$ m s^{-1}. The distribution of $\hat{\rho}_{hv}$ has a peak that is close to $\overline{\rho}_{hv}$ (which is < 1; see section 5d), but exhibits a very long tail at lower $\hat{\rho}_{hv}$, while there are no data with $\hat{\rho}_{hv} > 1$. Clearly, this distribution is not Gaussian and the negative skewness will negatively bias the mean of many $\hat{\rho}_{hv}$ samples compared to the true value of ρ_{hv}.

Fisher (1915) states that sample correlation coefficients ($\hat{\rho}$) of a true correlation coefficient ($\overline{\rho}$) calculated from a finite number of Gaussian random variables are skewed for $\overline{\rho} \neq 0$. However, the variable

$$\hat{F} = \frac{1}{2} \ln\left(\frac{1+\hat{\rho}}{1-\hat{\rho}}\right) \tag{3}$$

is Gaussian, with a mean of

$$\overline{F} = \frac{1}{2} \ln\left(\frac{1+\overline{\rho}}{1-\overline{\rho}}\right) \tag{4}$$

and standard error of

$$\sigma_F = \frac{1}{\sqrt{N-3}}, \tag{5}$$

where N is the number of independent samples used to calculate $\hat{\rho}$.

This is directly applicable to estimates of the radar copolar correlation coefficient, by realizing that the I and Q samples that are used to estimate ρ_{hv} are Gaussian random variables (Doviak and Zrnić 2006). Noting that $\hat{\rho}_{hv}$ in meteorological targets is always close to unity so that fractional changes in $(1 - \hat{\rho}_{hv})$ are always much greater than $(1 + \hat{\rho}_{hv})$, Eq. (3) can be written as

$$\hat{F} \approx \frac{1}{2}\ln 2 - \frac{\ln 10}{2}\log_{10}(1-\hat{\rho}_{hv}). \tag{6}$$

Since $\hat{F}$ is normally distributed, the quantity

$$\hat{L} = -\log_{10}(1-\hat{\rho}_{hv}) \tag{7}$$

is also normally distributed, with a mean of

$$\overline{L} = -\log_{10}(1-\overline{\rho}_{hv}) \tag{8}$$

and standard deviation of

$$\sigma_L = \frac{2}{\ln 10} \times \frac{1}{\sqrt{N_{IQ}-3}} \tag{9}$$

for $N_{IQ} \gg 3$, where N_{IQ} is the number of independent I and Q samples used to calculate $\hat{\rho}_{hv}$. Despite having similar characteristics, L is preferred over the use of F as it has the convenient property that $\rho_{hv} = 0.9$, 0.99, and 0.999 correspond to $L = 1$, 2, and 3, respectively, and therefore is more intuitive. Illingworth and Caylor (1991) plotted their $\hat{\rho}_{hv}$ data as $\log_{10}(1-\hat{\rho}_{hv})$ and their histograms also appear to be Gaussian in shape. Figure 3b illustrates the effect of the transform $\hat{L} = -\log_{10}(1-\hat{\rho}_{hv})$ on the distribution in Fig. 3a. The histogram is now symmetrical and bell shaped. A Gaussian curve with an equal mean and standard deviation to the $\hat{L}$ PDF is overplotted and is an excellent fit to the data, showing that the distributions are indeed Gaussian (and quantile–quantile plots, not shown here for brevity, confirm this).

To determine the number of independent I and Q samples, N_{IQ}, we consider the autocorrelation function for I and Q samples given by Doviak and Zrnić (2006):

$$R_{IQ}(nT_s) = \exp\left[-8\left(\frac{\pi\sigma_v nT_s}{\lambda}\right)^2\right], \tag{10}$$

where T_s is the time spacing between pulses of the same polarization and nT_s is the total time lag. Following the definition of Papoulis (1965), the time to independence for I and Q samples for large N_{IQ} can be shown to be

$$\tau_{IQ} = \frac{\lambda}{2\sqrt{2\pi}\sigma_v}, \tag{11}$$

where λ is the radar wavelength and σ_v is the Doppler spectral width. This is a factor of $\sqrt{2}$ smaller than the more often used time to independence for reflectivity samples. The number of independent I and Q pulses per ρ_{hv} sample can therefore be estimated by

$$N_{IQ} = \frac{T_{dwell}}{\tau_{IQ}} = \frac{2\sqrt{2\pi}\sigma_v T_{dwell}}{\lambda}, \tag{12}$$

where T_{dwell} is the dwell time.

The result [Eq. (9)] is significant as it shows that a confidence interval for any measurement of ρ_{hv} can be calculated solely in terms of the number of independent I and Q samples used to estimate it, which in turn can be readily estimated using the observed Doppler spectral width and Eq. (12). Furthermore, when multiple samples of $\hat{L}$ are averaged, no bias is introduced to estimates of $\hat{\rho}_{hv}$ because of the nonlinear transform. We expand this point in section 4.

To estimate confidence intervals for measurements of $\hat{\rho}_{hv}$, one must

- apply the transform $\hat{L} = -\log_{10}(1-\hat{\rho}_{hv})$,
- calculate the standard deviation of $\hat{L}$ using Eq. (9), and
- apply the inverse transform $1 - 10^{-(\hat{L}\pm\sigma_L)}$ to obtain upper and lower confidence intervals (where σ_L will contain the true value 68% of the time and $2\sigma_L$ will contain it 98% of the time).

More conveniently, one can simply transform $\hat{\rho}_{hv}$ data into $\hat{L}$ and use this for any subsequent analysis, with confidence intervals of $\hat{L} \pm \sigma_L$. This is the approach we follow in the rest of this paper. Although we are focusing on data with very high SNRs in this paper, the theory above should also be valid for weak SNR data, providing that noise introduced is also Gaussian in the I and Q samples.

This theoretical prediction was tested by comparing estimates of σ_L using data collected in homogeneous drizzle ($Z_{DR} < 0.1$ dB) with very good SNRs (> 40 dB). In drizzle, $\overline{L}$ is constant since the drops are spherical and, therefore, any variation σ_L is due to the finite N_{IQ}. Pulse-to-pulse H and V powers were recorded, and time series of various lengths between 0.2 and 30 s were constructed from these data and used to compute the

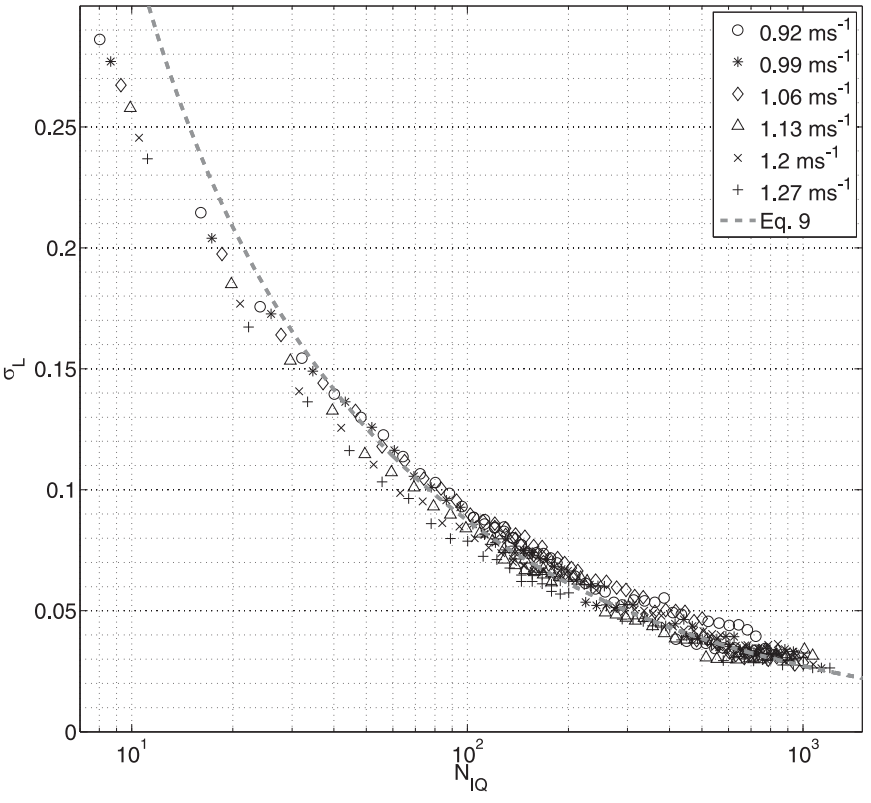

FIG. 4. The quantity σ_L as a function of the number of independent I and Q samples used to estimate L for high SNR measurements in drizzle ($Z_{DR} < 0.1$ dB; SNR > 40 dB) at 1203 UTC 6 Feb. Different markers correspond to different Doppler spectral widths.

corresponding N_{IQ} and $\hat{L}$ values. Data were binned by N_{IQ}, and the standard deviation σ_L was computed for each bin. Figure 4 shows how σ_L decreases as N_{IQ} is increased over more than two orders of magnitude. For $N_{IQ} \approx 10$, σ_L is slightly overestimated, and the data are in excellent agreement with the results predicted by Eq. (9) for $N_{IQ} > 30$.

4. Comparison with existing error statistics

We now compare these new error statistics with existing methods in the literature. From observations of ρ_{hv} in rain, the bright band, and ice, Illingworth and Caylor (1991) derived empirically the relationship between their mean $\hat{\rho}_{hv}$ estimates and their standard deviation:

$$\sigma^{IC}_{\rho_{hv}} \simeq \frac{1.25(1-\hat{\rho}_{hv})}{\sqrt{n}}, \tag{13}$$

where n is the number of 0.2-s time series they used to estimate the mean ρ_{hv}. Using a linear perturbation technique, Torlaschi and Gingras (2003) derive the following equation for the standard deviation of a ρ_{hv} measurement:

$$\sigma^{TG}_{\rho_{hv}} = \frac{1-\overline{\rho}^2_{hv}}{\sqrt{2N_I}}, \tag{14}$$

where N_I is the number of independent radar reflectivity samples used for its estimation. Note that $\overline{\rho}_{hv}$ in Eq. (14) is the true correlation coefficient one is attempting to measure (rather than the measured value, $\hat{\rho}_{hv}$). This equation represents the standard deviation for infinite SNR conditions and is valid for simultaneous or accurately interpolated H and V sampling. Neither one of these techniques is ideal, relying on either knowing a priori the true correlation coefficient one is attempting to measure (Torlaschi and Gingras 2003) or a number of time series (Illingworth and Caylor 1991) and not the number of independent pulses. It is not possible to compare the method of Illingworth and Caylor (1991) with our proposed method because σ_v for their data is unknown, and therefore the number of independent pulses in their time series cannot be quantified. Figure 5a shows the errors on $\hat{\rho}_{hv}$ calculated using our new method compared to those calculated using the linear perturbation method of Torlaschi and Gingras (2003) as a function of N_{IQ} in rain ($\overline{\rho}_{hv} = 0.98$). The magnitudes of the upper confidence bounds are largely similar; however,

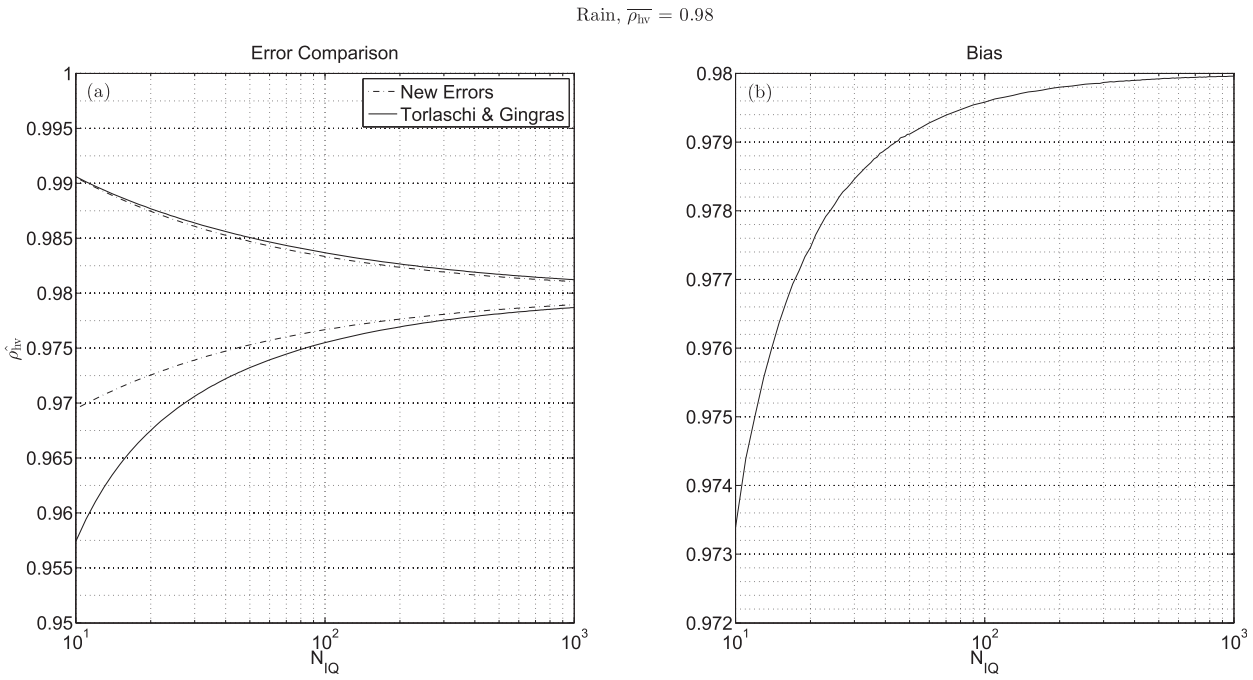

FIG. 5. (a) A comparison of the confidence intervals calculated using the new method and that of Torlaschi and Gingras (2003) in rain ($\overline{\rho}_{hv} = 0.98$) and (b) the bias introduced by averaging $\hat{\rho}_{hv}$ instead of $\hat{L}$, as a function of N_{IQ}. For all N_{IQ}, the lower confidence interval is higher for the Torlaschi and Gingras (2003) method, particularly for lower N_{IQ}, because of the asymmetric nature of the confidence intervals on ρ_{hv} using the new method. Averaging $\hat{\rho}_{hv}$ and not $\hat{L}$ for small N_{IQ} can lead to a large bias.

for all N_{IQ} the lower confidence interval is higher for Torlaschi and Gingras (2003) (i.e., smaller deviations from $\overline{\rho}_{hv}$ are predicted), because of the asymmetric nature of the new confidence intervals on $\hat{\rho}_{hv}$. The largest difference is for small N_{IQ}. As N_{IQ} increases, both the upper and lower confidence intervals for each method converge. Although Fig. 5a serves as a useful illustration of the difference between the methods, they are not strictly comparable in practice: the error calculation of Torlaschi and Gingras (2003) relies on knowledge of $\overline{\rho}_{hv}$, which in reality is unknown. Conversely, the new method requires no a priori knowledge of $\overline{\rho}_{hv}$ and, so, is of much greater practical use.

Figure 5b illustrates the theoretical bias introduced by averaging many short samples of $\hat{\rho}_{hv}$, rather than $\hat{L}$, in rain ($\overline{\rho}_{hv} = 0.98$). This bias is significant for small N_{IQ}. For example, when $N_{IQ} = 10$, the bias on $\hat{L}$ is 0.1, which is significant for the purpose of estimating μ in rainfall; this bias in L could lead to an underestimate of μ of approximately 8 at $Z_{DR} = 2$ dB (see Fig. 8). It is not important whether spatial or temporal averaging is used to increase the number of independent I and Q samples, as long as $\overline{\rho}_{hv}$ does not vary substantially over the scales considered.

In summary, confidence intervals that rely on the linear perturbation method overestimate the precision of ρ_{hv} measurements, and require knowledge of the true ρ_{hv} one is attempting to measure. Fundamentally, failure to use the transform L when averaging short time series will lead to significant biases in correlation coefficient estimates. This is particularly important for operational ρ_{hv} applications that typically use very short dwell times (discussed in section 8a), and would lead to a significant bias in retrievals of μ in rain.

5. Practical measurement of ρ_{hv}

To fully exploit our new error estimates, and retrieve rain DSDs, some practical considerations for the measurement of ρ_{hv} must first be considered.

a. *Effect of alternate sampling*

When estimating the correlation coefficient, the nonsimultaneous transmission and reception of H and V pulses must be accounted for. Assuming a Gaussian autocorrelation function to correct for this staggered sampling (Sachidananda and Zrnić 1989) can lead to unphysical samples where $\hat{\rho}_{hv} > 1$ (Illingworth and Caylor 1991). In our analysis, we employ a cubic polynomial interpolation to obtain H and V power estimates at the intermediate sampling intervals (Caylor 1989), which is very effective. We find that the interpolation scheme works well: for drizzle with $\overline{L} = 2.4$, we observe

that average values of $\hat{L}$, binned by σ_v, are constant to within ± 0.02 as σ_v varies between 0.1 and 2 m s^{-1}. This is evidence of successful interpolation, since there is no systematic trend to lower L values at higher spectral widths.

b. Signal-to-noise ratio

The addition of noise to the received signals acts to reduce the correlation between the H and V time series. The reduction factor f has been shown (Bringi et al. 1983) to vary predictably as

$$f = \frac{1}{\left(1 + \frac{1}{\mathrm{SNR}_H}\right)^{1/2}\left(1 + \frac{1}{\mathrm{SNR}_V}\right)^{1/2}} \qquad (15)$$

for simultaneous (or accurately interpolated) H and V sampling, where SNR_H and SNR_V are the signal-to-noise ratios for the H and V polarizations, respectively. This was verified by Illingworth and Caylor (1991) with measurements of ρ_{hv} in drizzle. While it is in principle possible to correct for the presence of noise using this equation, because of the high degree of precision required in this work, only data with SNR > 34 dB are included in our analysis, which corresponds to a maximum achievable ρ_{hv} measurement of 0.9996. However, instrumental effects (described in section 5d below) will have the same effect of adding uncorrelated noise, and so in practice this maximum value is never reached.

c. Effect of phase error

To avoid a bias in $\hat{\rho}_{\mathrm{hv}}$ due to random phase error from our magnetron system (Liu et al. 1994), we cross correlate the power of the received echoes as opposed to the complex I and Q signals, and take the square root, following Illingworth and Caylor (1991).

d. Instrumental effects

Even in drizzle with very high SNR, antenna imperfections and other effects such as irregular magnetron pulse timing and pulse shape reproducibility will cause measured ρ_{hv} to always be <1 (Illingworth and Caylor 1991; Liu et al. 1994), as effectively they cause the H and V pulses to sample slightly different volumes. Here, we propose a method for quantifying and accounting for this bias, analogous to the SNR factor [Eq. (15)] suggested by Bringi et al. (1983). We consider the H and V echoes to consist of two parts: a common sample volume and parts of each sample volume, which are unique to a particular polarization. By treating the former as "signal" and the latter as unwanted "noise," we obtain an equation similar to Eq. (15). Full details are provided in the appendix. The practical upshot is that the measured ρ_{hv} is the true ρ_{hv} multiplied by some dimensionless factor, $f_{\mathrm{hv}}^{\mathrm{max}}$, relating to how well matched the H and V sample volumes are. For spherical drops, $\overline{\rho}_{\mathrm{hv}}$ should be unity. The estimates of $\overline{\rho}_{\mathrm{hv}}$ for all such data should therefore be equal to $f_{\mathrm{hv}}^{\mathrm{max}}$. When comparing observations with simulated ρ_{hv}, we multiply each of the predicted values by $f_{\mathrm{hv}}^{\mathrm{max}}$ so that they are directly comparable to the observations. Values of ρ_{hv} have been measured in drizzle ($Z_{\mathrm{DR}} < 0.1$ dB) for a large number of samples on several days. Typically, $f_{\mathrm{hv}}^{\mathrm{max}}$ is ≈ 0.996, but varies by ± 0.001 from day to day, which we suggest is the result of slightly irregular magnetron pulse timing and shape reproducibility for the CAMRa system, which may be temperature dependent. For this reason, $f_{\mathrm{hv}}^{\mathrm{max}}$ has been determined individually for each case.

6. Using L and Z_{DR} to estimate μ in rainfall

We now attempt to use our high-precision measurements of L to retrieve μ estimates in rainfall. The independence of (D_0, μ) and (L, Z_{DR}) on the drop number concentration means that a single L and Z_{DR} observation pair corresponds to a unique D_0 and μ value. To forward model L and Z_{DR} for various gamma distributions, we must first assume an appropriate drop shape model.

a. Mean drop shapes

There are numerous drop shape parameterizations in the literature. Here, we examine drop axis ratios and diameters from the recent experiments of Thurai and Bringi (2005), Szakáll et al. (2008), and the fourth-order polynomial fit to many experiments given by Brandes et al. (2002). Figure 6a shows the mean axis ratio as a function of drop diameter, for each of these models. The Thurai and Bringi (2005) data suggest that mean drop shapes are slightly prolate for $D < 1$ mm, although it is in the margin of measurement error that the drops are spherical (Beard et al. 2010). Since it is known that drops become spherical as their diameter tends to 0 mm because of surface tension, our fit to the data is adapted so that drops < 1 mm are precisely spherical.

To choose the best mean drop shape model, a 5-h dwell was made with CAMRa at a 1.5°-elevation angle over a nearby Joss–Waldvogel RD-80 impact disdrometer (approximately 7 km away) in a frontal rainband on 25 April 2014. The disdrometer measures drop sizes in 127 size bins from 0.3 to 5.0 mm. The instrument is regularly calibrated by the manufacturer and rain rates estimated with this instrument agree very well with those from a collocated rain gauge. Radar measurements of Z_{DR} are calibrated regularly (to within ± 0.1 dB) by making observations of drizzle (low Z),

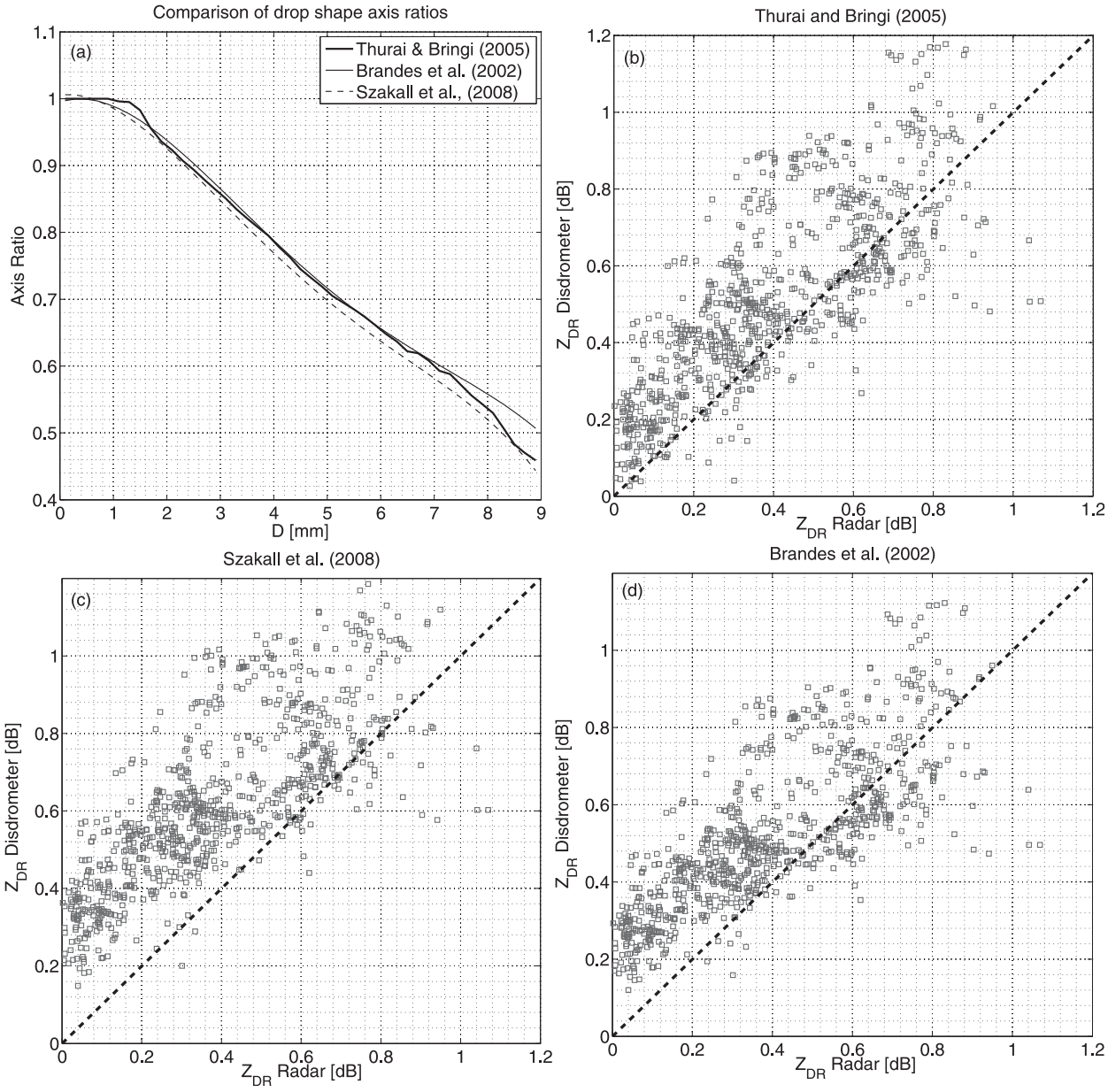

FIG. 6. (a) Comparison of mean drop axis ratios as a function of equivalent drop diameter D from recent experiments of Thurai and Bringi (2005), Szakáll et al. (2008), and the fourth-order polynomial fit of older experimental data constructed by Brandes et al. (2002). The model of Thurai and Bringi (2005) has been adapted so that drops are spherical for $D < 1$ mm. Disdrometer Z_{DR} is calculated using the drop shape models of (b) Thurai and Bringi (2005), (c) Szakáll et al. (2008), and (d) Brandes et al. (2002) from a 5-h dwell over a nearby Joss–Waldvogel RD-80 impact disdrometer (approximately 7 km away) in a frontal rainband on 25 Apr 2014. The time resolution of the radar measurements was decreased to 30 s to match the integration time of the disdrometer. At a 1.5°-elevation angle, the radar was sampling rain at a height of approximately 183 m above the disdrometer. The dashed line is a 1:1 line. The smallest biases are achieved with the Thurai and Bringi (2005) model, especially for smaller Z_{DR}, suggesting that these shapes best represent those of natural raindrops. Therefore, this model is chosen for the analysis.

which we know to have a Z_{DR} value of 0 dB. The range resolution of the radar measurements is 75 m, and is averaged to 30 s to match the integration time used by the disdrometer to estimate the DSD parameters. At this elevation angle, the radar was sampling rain at a height of 183 m above the disdrometer. Figures 6b–d show the observed radar measurement from the closest gate to the disdrometer, as well as the corresponding disdrometer Z_{DR} values calculated using the Thurai and Bringi (2005), Szakáll et al. (2008), and Brandes et al. (2002) drop shape

models, respectively. The Szakáll et al. (2008) axis ratios are systematically smaller compared to both of the other models for almost all D. Using this model makes the disdrometer estimates of Z_{DR} always larger than the radar estimates. Thurai and Bringi (2005) and Brandes et al. (2002) agree for $D = 2$–7 mm, after which the axis ratios of Thurai and Bringi (2005) are closer to those of Szakáll et al. (2008). Therefore, the radar and disdrometer Z_{DR} values for the Thurai and Bringi (2005) and Brandes et al. (2002) models largely agree, apart from $Z_{DR} \lesssim 0.4$ dB. The largest difference between these models occurs for $D < 2$ mm. Here, Szakáll et al. (2008) and Brandes et al. (2002) predict more oblate drops than do Thurai and Bringi (2005).

The Szakáll et al. (2008) model produces the largest radar–disdrometer overall bias of ≈0.23 dB. The biases from Brandes et al. (2002) for Z_{DR} bins of 0.2, 0.4, and 0.6 dB (±0.1-dB bin width) are 0.09, 0.16, and 0.13 dB, respectively. For the Thurai and Bringi (2005) model, they are only 0.04, 0.08, and 0.09 dB, respectively, and are very similar to results found by Brandes et al. (2002) at higher Z_{DR}. These reduced biases at low Z_{DR} suggest that the experimental results of Thurai and Bringi (2005) best represent natural raindrop shapes. We therefore chose this model in our analysis. It is unclear why the very small residual difference between radar and disdrometer estimates of Z_{DR} using the Thurai and Bringi (2005) shape model is observed. Some possible explanations are that the radar calibration is slightly off causing a systematic underestimation, the small sampling volume of the disdrometer could be biasing Z_{DR}, or there could be residual error in the mean drop shape model. However, this very small difference is unimportant for the retrievals that follow.

b. *Drop oscillations*

Drop oscillations increase the variety of shapes within a radar pulse volume at any given time. This means that the $\overline{L}$ we are attempting to estimate will be lower than that predicted by modeling only the mean drop axis ratios for drops of a given size. To account for this, we must parameterize these drop oscillations. In the Thurai and Bringi (2005) experiment, artificial raindrops were created from a hose and allowed to fall 80 m from a bridge before drop axis ratio and counts were measured with a 2DVD on the valley floor. This fall distance is more than sufficient to allow the drops to achieve steady-state oscillations, and so the standard deviations of axis ratios measured in this experiment are interpreted as drop oscillation amplitudes. However, the large standard deviations of the axis ratios for $D < 2$ mm are likely artificial, caused by the finite resolution of the 2DVD instrument (Beard et al. 2010). Since drop oscillations are thought to originate from vortex shedding (Beard et al. 2010), which increases as a function of drop size, the magnitude of the oscillations should decrease eventually to zero as the drop diameter tends to 0 mm. Beard and Kubesh (1991) suggest that resonant drop oscillations occur for drop sizes between 1.1 and 1.6 mm; however, more recent measurements from the University of Mainz wind tunnel show that amplitudes of the axis ratios for these drop sizes were less than 0.025 (Szakáll et al. 2010). For this reason, the polynomial fit to oscillation amplitude data from the Mainz wind tunnel (Szakáll et al. 2010) is used for $D < 2$ mm, which has the desired reduction in oscillation amplitude for small drops.[1] For $D > 2$ mm, we revert to the more statistically robust drop oscillations from Thurai and Bringi (2005). Since the oscillations are aerodynamically induced, with an amplitude only a function of the drop size, they should not vary with environmental conditions. In our analysis, the oscillations were included by integrating over Gaussian PDFs of axis ratios (Thurai and Bringi 2005) in our Gans theory computations. Figure 7 shows the effect of oscillations on computed L and Z_{DR} for values of $\mu = -1$ (solid lines) and $\mu = 16$ (dashed lines). Including drop oscillations for the purpose of estimating μ becomes increasingly important with increasing Z_{DR}; the difference between L at $\mu = 16$ computed with and without oscillations is as large as an equivalent change in μ of ≈ 8. We find that the modification of the oscillation magnitudes for drop diameters < 2 mm has a relatively small impact (<0.01) on predicted L for Z_{DR} larger than 0.8 dB where we attempt retrievals of μ. However, we find that the use of Szakáll et al. (2010) oscillations for all drop diameters has a large impact on predicted L values (for $\mu = -1$, L is approximately 0.1 lower). This is potentially important for retrievals of μ.

Comparatively large-amplitude (but short lived, lasting less than approximately 0.4 s) collision-induced oscillations can also occur (Szakáll et al. 2014). Rogers (1989) estimate that the collision rate for an average raindrop in a 55-dBZ rain column is approximately 1 min^{-1}. This would imply that raindrops (even in very heavy rainfall) spend an almost negligible fraction of time (approximately 0.5%) affected by collision-induced oscillations. Raindrop clustering increases the likelihood of these collisions (Jameson and Kostinski 1998). For rain rates of around 10 mm h^{-1} (comparable to those presented in the following case studies), McFarquhar (2004)

[1] Equation (1) in Szakáll et al. (2010) does not agree with the fit in Fig. 3 (black line). By digitizing the Mainz wind tunnel data, we calculate that their Eq. (1) should in fact be $1.8 \times 10^{-3} D_0^2 + 1.07 \times 10^{-2} D_0$.

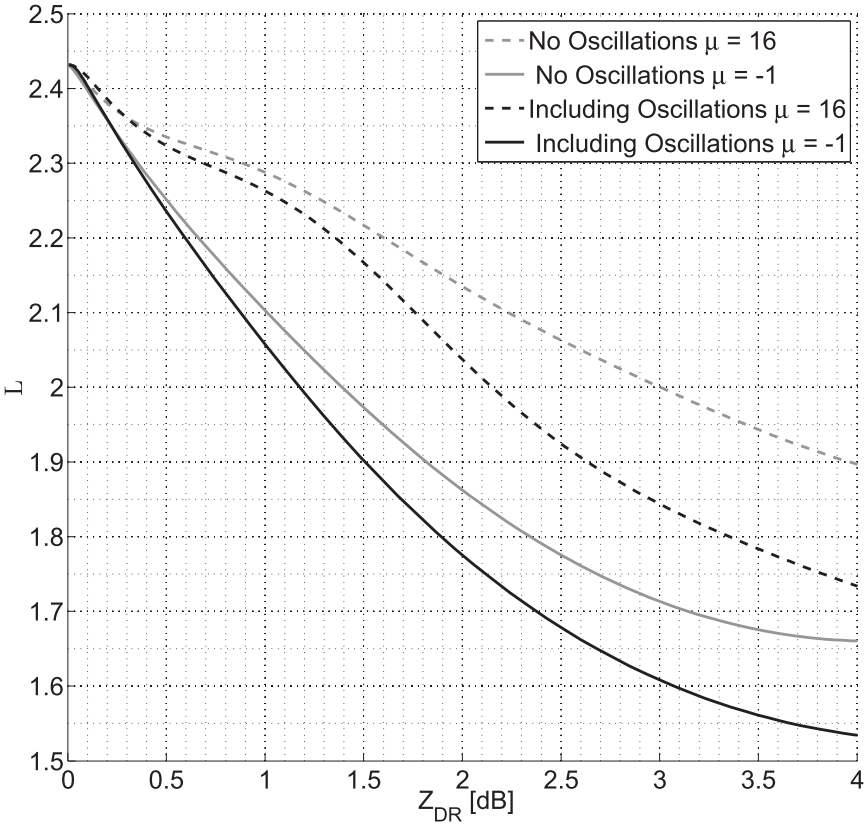

FIG. 7. Predicted L and Z_{DR} values for gamma distributions of $\mu = -1$ (solid) and 16 (dashed) with no oscillations (gray) and including oscillations (black). The inclusion of drop oscillations is crucial to the interpretation of the L and Z_{DR} measurements. The f_{hv}^{max} is assumed to be 0.9963 to match the case study in section 7.

estimate the collision rate to be about 5 min^{-1}, implying drops are affected only 3% of the time. For very large rain rates (100 mm h^{-1}), this fraction increases to 6% as the collision rate approximately doubles to 10 min^{-1}. Consequently, their impact on L measurements is likely to be small and can be ignored, other than for exceptional rain rates (Thurai et al. 2013).

Figure 8 shows how L varies as a function of Z_{DR} for gamma distributions with $\mu = -1$, 0, 2, 4, 8, 12, and 16 computed using Gans theory with the drop shape and oscillation model discussed above. Note that lines of constant μ diverge with increasing Z_{DR}. For $Z_{DR} \gtrsim 0.5$ dB, it becomes possible to distinguish μ, given the typical error on an L measurement (shown in Fig. 9).

7. Case studies of μ retrieval

We now estimate μ using measurements of L and Z_{DR} for stratiform rain case studies on 31 January, 25 April, and 25 November 2014, and a convective case study on 22 May 2014. Typical rain rates for each of these case studies can be found in Table 1. Dwells were made at an elevation angle of 1.5°. Strict data quality filters were applied: SNR $>$ 34 dB, linear depolarization ratio (LDR) < -27 dB (close to the limit of cross-polar isolation) to ensure no melting particle contamination or ground clutter, and range $>$ 5 km to avoid near-field effects. Theoretical L and Z_{DR} were computed using Gans theory using the drop shape and oscillation model discussed in section 6 (see Fig. 8). Observations were averaged from 10 to 30 s and from range gates of 75 to 300 m to increase the measurement precision of L. At each gate, the most likely pair of μ and D_0 given the observed L and Z_{DR} values was obtained by selecting the closest point in a lookup table of gamma DSD calculations. Figure 9a shows the observed L binned every 0.02 and Z_{DR} binned every 0.05 dB for the example of 25 November 2015. Overlaid are lines of constant $\mu = -1$, 0, 2, 4, 8, 12, and 16. Figure 9b is the same distribution normalized to sum to 1 for each Z_{DR} bin. The f_{hv}^{max} on this day was calculated to be 0.9963 (see section 5d). The observations of L and Z_{DR} are generally

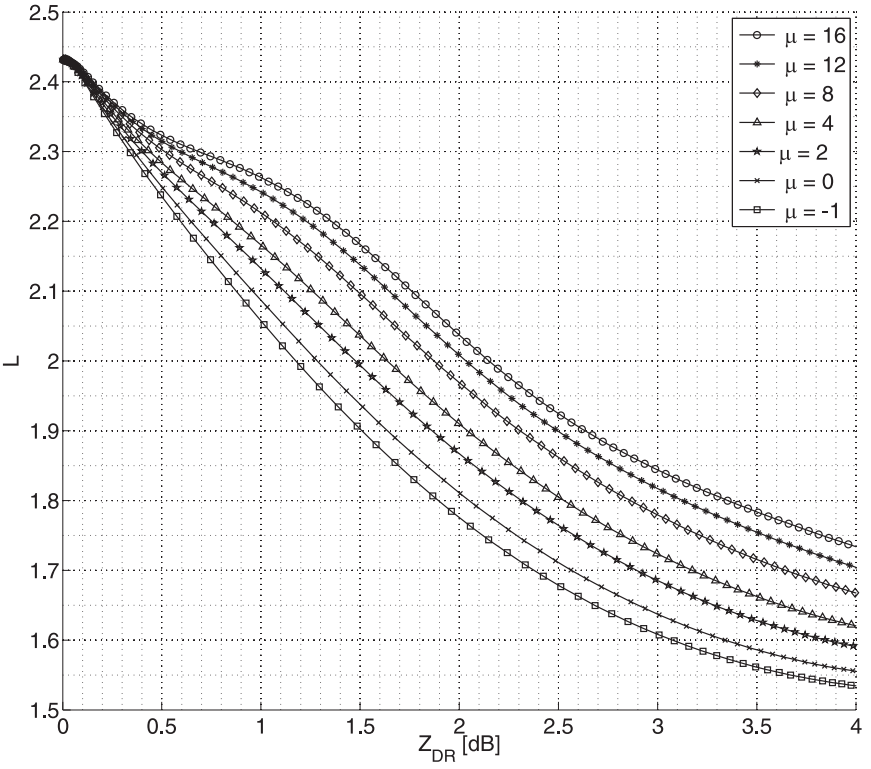

FIG. 8. Theoretical L and Z_{DR} results computed using Gans theory for gamma distributions with $\mu = -1, 0, 2, 4, 8, 12$, and 16, using Thurai and Bringi (2005) mean drop axis ratios and the oscillation model described in section 6b. The precision of L required to estimate μ decreases as Z_{DR} increases. The f_{hv}^{max} is assumed to be 0.9963 to match the case study in section 7.

well contained within the expected range. The median error on $\hat{L}$ is $\sigma_L \approx 0.025$, and is shown as a representative error bar in Fig. 9. A comparison of these data with disdrometer measurements from Williams et al. (2014) is included. In this experiment, the mass spectrum mean diameter D_m and mass spectrum standard deviation σ_m were measured using a 2DVD. A σ_m–D_m fit was derived from 18 969 measurements of 1 min drop spectra (which can readily be converted to a μ–D_0 fit). This was in turn used to predict an L–Z_{DR} relationship, shown by the gray dashed line. Both L and Z_{DR} were also predicted using the proposed μ–Λ relationship of Cao et al. (2008), which is also derived from a 2DVD, where

$$\Lambda = \frac{3.67 + \mu}{D_0}. \tag{16}$$

This is shown by the black dashed line.

The median and interquartile range of retrieved μ per Z_{DR} bin for this day are shown in Fig. 10. The median retrieved μ is 5 at $Z_{DR} = 0.8$ dB, increasing to 8 for $Z_{DR} = 1.6$ dB. There is significant spread in retrieved μ values, containing contributions from measurement uncertainty on L, as well as true microphysical variability. The impact of changes in L on retrieved μ is nonlinearly related to μ; σ_L contributes more to retrieved μ variability for more monodispersed (higher μ) DSDs than for more polydispersed (lower μ) DSDs. Conversely, the contribution of σ_L to retrieved μ variability decreases as Z_{DR} increases, as the dual-polarization signature is larger and μ is more easily distinguishable (see Fig. 8). To estimate the contribution that the uncertainty on L measurements makes to this observed variability, μ was retrieved using the median $L \pm$ the representative uncertainty depicted in Fig. 9. This was then compared with the interquartile range of the retrieved μ for each Z_{DR} bin. For Z_{DR} bins of 0.8, 1, 1.2, 1.4, and 1.6 dB, we estimate that 88%, 66%, 32%, 31%, and 27% of the variability, respectively, can be attributed to σ_L. For $Z_{DR} > 1$ dB, most of the variability seen in Fig. 10 can be attributed to true microphysical variability.

Figure 11 shows a comparison with retrieved μ for all of the case studies collected. Each of the dwells in

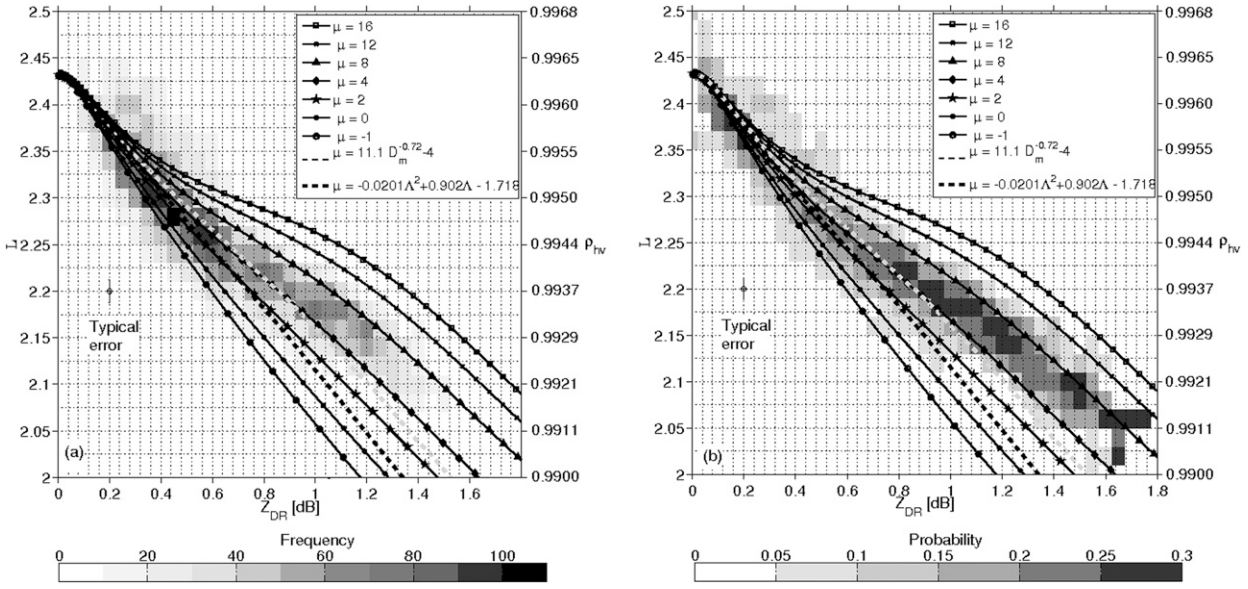

FIG. 9. (a) The 2D PDF of L and Z_{DR} observations, and (b) the normalized 2D PDF such that the distribution equals 1 for each Z_{DR} bin for observations of L and Z_{DR} collected from dwells on 25 Nov 2014. Here, L is binned every 0.02, and Z_{DR} is binned every 0.05 dB. Overplotted are theoretical L and Z_{DR} values computed using Gans theory for gamma distributions of $\mu = -1, 0, 2, 4, 8, 12$, and 16. Typical errors on L and Z_{DR} are shown as error bars; the error on Z_{DR} is very small. The gray dashed line indicates the predicted L and Z_{DR} observations using DSD parameters from the power-law fit to disdrometer measurements in Williams et al. (2014). The black dashed line indicates the predicted L and Z_{DR} observations using the μ–Λ relationship of Cao et al. (2008). The f_{hv}^{max} for this day is measured to be 0.9963.

January, April, and November was made in stratiform rain, whereas the May case study contains dwells from convective rain. Overlain are predicted mean μ values (solid gray) and upper and lower bounds that contain 55% of the measurements (dashed gray) of Williams et al. (2014) as a function of Z_{DR} from the disdrometer measurements. The solid black line shows the predicted μ–Z_{DR} relationship using the μ–Λ relationship of Cao et al. (2008). There is a large spread in the radar-retrieved median μ values from case to case. Each median μ estimate is from a very large number of retrieved μ estimates, such that the standard error is smaller than the markers themselves, and so is not shown. The values of retrieved μ in January are approximately 0, close to an exponential DSD for all Z_{DR} smaller than 1.1 dB. This is below the value predicted by Williams et al. (2014) but agrees well with μ predicted by Cao et al. (2008). Interestingly, the case studies of April and November show μ increasing with Z_{DR} between 0.5 and 1.5 dB, compared to the trend seen by Williams et al. (2014) and Cao et al. (2008) toward an exponential DSD. The retrieved median μ values from the May case study, although agreeing with the decreasing trend with Z_{DR}, are significantly above the Cao et al. (2008) predictions and the upper bound of μ from Williams et al. (2014). Our retrieval suggests that, in this case, the rain rate would be overestimated by almost 2 dB if an exponential DSD or the fit of Cao et al. (2008) is assumed. Whereas the μ values are not outside the full range of data measured by Williams et al. (2014), the use of the proposed μ–D_m relationship would cause an overestimate of about 1 dB (see Fig. 1).

8. Discussion

Our retrievals of μ made using ρ_{hv} and Z_{DR} are typically larger than the radar estimates of μ of between 1 and 3 by Thurai et al. (2008) and of between 0 and 2 by Illingworth and Caylor (1991). Perhaps this is not surprising, given that the imperfect collocation of the H and V sample volumes was unaccounted for, and their $\hat{\rho}_{hv}$ would have been biased low as a result of averaging ρ_{hv} rather than L, both of which are accounted for in our data. Furthermore, Illingworth and Caylor (1991) do not

TABLE 1. Typical rain rates for each of the case studies, calculated from disdrometer measurements (April) and radar-retrieved N_0, D_0, and μ values (January, May, and November).

Date (2014)	Typical R (mm h^{-1})	Peak R (mm h^{-1})
31 Jan	1–3	8
25 Apr	2–3	7
22 May	2–7	>30
25 Nov	2–5	10

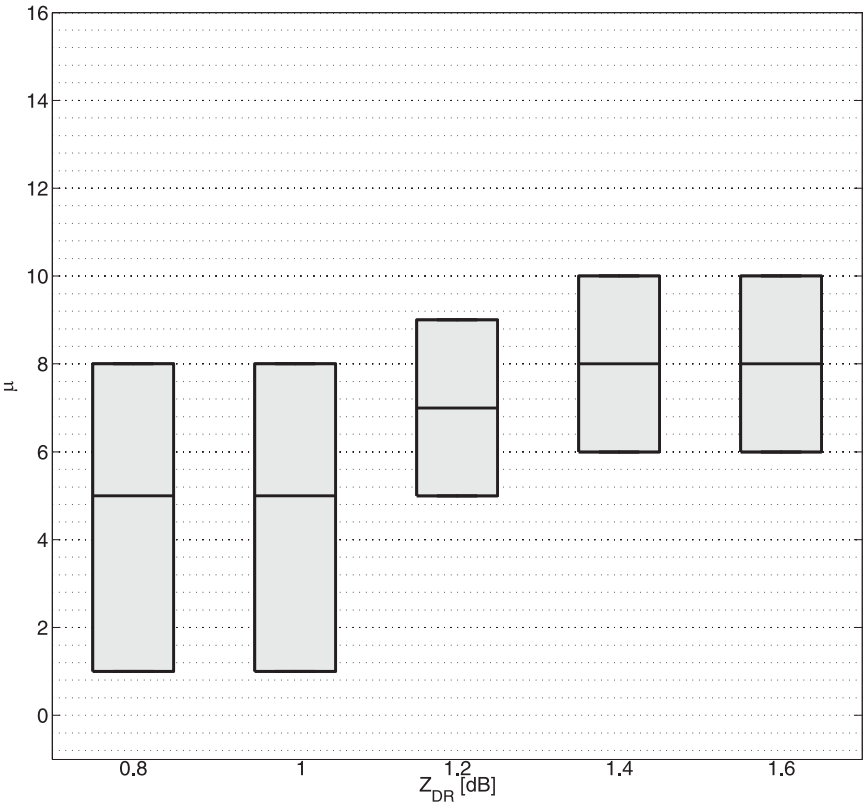

FIG. 10. Box plot of retrieved μ as a function of Z_{DR} for Z_{DR} bins of 0.2 dB on 25 Nov 2014, showing the median and interquartile range of the data.

include drop oscillations in their retrievals, which will have led to a significant underestimate of μ. Whereas there is some agreement of the magnitudes of μ for $Z_{DR} < 1$ dB with predicted Williams et al. (2014) and Cao et al. (2008) values, the apparent opposite trend toward more monodisperse distributions is consistent among three of the four case studies. For the retrieved μ to agree with the trend predicted by Williams et al. (2014) or Cao et al. (2008), a reduction in the drop oscillation amplitudes for smaller drops would be required so that predicted L values are higher. However, this would not explain the difference between the May retrieval results and the predicted μ from disdrometer measurements; we estimate that it would require oscillations that are at least an order of magnitude *larger* to bring these median μ estimates into agreement with Williams et al. (2014) or Cao et al. (2008). An incorrect parameterization of the drop oscillations alone is unlikely to be able to account for the disagreement with Williams et al. (2014) and Cao et al. (2008); however, to better establish the accuracy of the technique, a better quantification of raindrop oscillations is desirable.

The μ estimates derived using radar are sensitive to higher moments of the DSD, whereas disdrometer estimates tend to use lower moments of the DSD (Cao and Zhang 2009). This could be partly responsible for the differences between the radar- and disdrometer-estimated μ values. If the DSD shape is not perfectly described by Eq. (1), the "effective" μ that is derived may be different even if the underlying DSD shape is the same. It is also possible that what we have captured is simply the natural variability of the DSD in different types of rainfall (i.e., convective and stratiform), and there is not a universal μ–D_m relationship. More case studies are needed to gather a statistical understanding of the behavior of μ using this retrieval method.

Implications for the operational use of L

Operational radar networks favor the use of rapid scan rates to maximize sample frequency and total sample volume. For Met Office radars observing rain with 1 m s^{-1} Doppler spectral width, each gate contains $N_{IQ} \approx 11$ ($\sigma_L \approx 0.3$). Clearly, many more N_{IQ} are needed than are available for individual gate estimates of μ. Greater measurement precision can be achieved by averaging (with the confidence interval computed using the aggregated number of independent I and Q samples), and assuming μ is spatially conserved over the

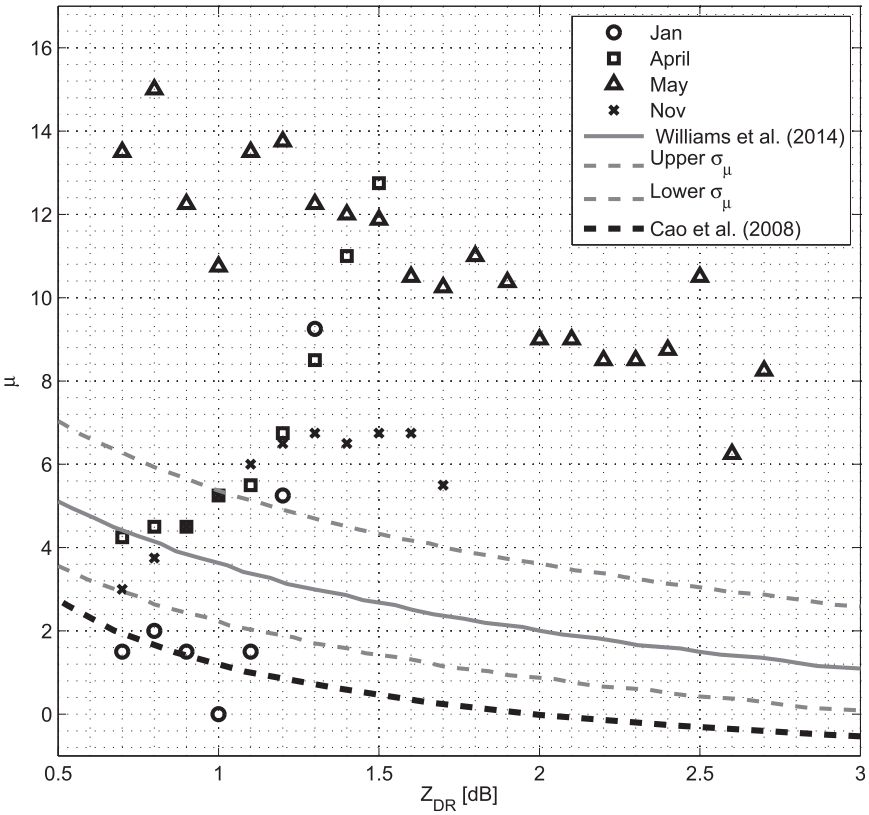

FIG. 11. Median retrieved μ as a function of Z_{DR} for Z_{DR} bins of 0.1 dB for case studies of 31 Jan, 25 Apr, 22 May, and 25 Nov 2014. The solid gray line is the predicted μ as a function of Z_{DR} from the power-law fit to the disdrometer measurements of Williams et al. (2014), and σ_μ corresponds to the dashed gray upper and lower bounds that contain 55% of the data. The solid black line shows the predicted μ–Z_{DR} relationship using the μ–Λ relationship of Cao et al. (2008).

chosen averaging area. To obtain a μ estimate over approximately 1 km^2, for example, would require the averaging of two rays and 10 gates (at a range from the radar of 30 km); this L estimate would be calculated using $N_{IQ} = 220$ ($\sigma_L \approx 0.058$). Whereas this may not be sufficient to distinguish μ to as high a resolution as our retrieval (which uses long dwells and $N_{IQ} > 1000$), this will at least be able to decipher whether μ is "high" or "low." Practically, as illustrated in Fig. 1, this may be all that is necessary to offer improved rain-rate estimates; it is relatively unimportant whether μ is 8 or 16, but it is very important to know if it is 0 or 4. Therefore, this method could (with sufficient care to ensure only rain echoes and good SNR) allow for improved rain rates using Z, Z_{DR}, and L when compared with only Z and Z_{DR}.

For the typical σ_L used in these calculations, we can approximate the error on the retrieved rain rate by considering the contribution of σ_L to the uncertainty in μ. For a "typical" μ of 6, the range of retrieved μ is about ± 4. By referring to Fig. 1, we can see that this corresponds to a difference in the rain rate of ± 0.5 dB, or $\pm 12.5\%$. The impact of uncertainty in μ on the rain rate is almost constant for all Z_{DR} (each of the μ lines are approximately parallel in Fig. 1 for $Z_{DR} \gtrsim 0.5$ dB). Therefore, this error will decrease for higher rain rates as the contribution of σ_L to the uncertainty in μ decreases as a function of Z_{DR}.

9. Conclusions

In this paper, a new variable, $L = -\log_{10}(1 - \rho_{hv})$, is defined that is Gaussian distributed with a width predictable by the number of independent I and Q samples, which in turn can be estimated using the Doppler spectral width. This allows, for the first time, the construction of rigorous confidence intervals on each ρ_{hv} measurement. The predicted errors using this new method were verified using high-quality measurements in drizzle from the Chilbolton Advanced Meteorological Radar.

The proposed method is of much greater practical use than the linear perturbation error estimation method, as it does not require knowledge of the unknown "true" ρ_{hv} that one is trying to estimate. The method works for both simultaneous or accurately interpolated alternate sampling. However, it does not work for alternate estimators, which rely on the Gaussian autocorrelation function to estimate the zero-lag correlation between H and V pulses (Sachidananda and Zrnić 1989), where ρ_{hv} estimates can be >1.

A new technique to account for the imperfect collocation of H and V sampling volumes on ρ_{hv} measurements is presented. The impact of drop oscillations on the observed L measurements was shown to be significant; omitting oscillations from our Gans simulations leads to an underestimate of retrieved μ of approximately 8. We further show that failure to use L over ρ_{hv} measurements when averaging can lead to a significant bias low in ρ_{hv} estimates (and consequently μ), particularly for very short dwell times such as those used operationally.

High-precision measurements of L and Z_{DR} in rainfall are then used to estimate μ in the gamma DSD for four case studies. We find that our estimates of μ in stratiform rain somewhat agree in magnitude with those from disdrometer studies for small Z_{DR}, but there appears to be a tendency toward more monodisperse DSDs between Z_{DR} = 0.8 and 1.5 dB, unlike the trend toward an exponential distribution suggested by disdrometer measurements. The convective case study does display this trend toward lower μ as Z_{DR} increases, but the magnitude of μ remains much larger than predicted by disdrometer measurements. If true, this would lead to overestimates of retrieved rain rate by approximately 1 dB if the μ–D_m relationship of Williams et al. (2014) is used, or 2 dB if an exponential distribution or the μ–Λ relationship of Cao et al. (2008) is used. We find that the μ retrieval exhibits sensitivity to the choice of the drop oscillation model. A better understanding of raindrop oscillations would be useful to fully establish the accuracy of our retrieval technique.

The variability in our radar-retrieved μ could simply be the natural variability of the DSD between convective and stratiform rainfall; there may not be a universal μ–D_0 relationship. More case studies are desirable to investigate this further.

The μ retrieval technique employed here offers improvements over the radar estimates of Illingworth and Caylor (1991) and Thurai et al. (2008). Illingworth and Caylor (1991) did not take into account the imperfect collocation of the H and V sample volumes on measurements of ρ_{hv}, the effect of drop oscillations, or the fact their ρ_{hv} estimates would be biased low by averaging short time series. Each of these effects would cause μ to be underestimated. The same is true of Thurai et al. (2008); however, drop shapes measured by 2DVD measurements include oscillations, and so are included in their μ estimates.

The new error statistics of ρ_{hv} presented here could aid operational applications that require uncertainty on $\hat{\rho}_{hv}$ to be quantified, or use averages of $\hat{\rho}_{hv}$. The use of L operationally to retrieve μ is limited by the use of rapid scan rates and the corresponding few independent I and Q samples. However, assuming that μ is a smoothly varying parameter, averaging L could help improve rain-rate retrievals; the uncertainty on operationally retrieved rain rates using the retrieval technique presented here is estimated to be approximately ±12.5%. Practically, retrieved rain rates are less affected by changes in higher values of μ than by changes in lower values. Therefore, operationally, simply being able to distinguish between regions of "high" and "low" μ with L could be sufficient to provide an improvement over existing Z–Z_{DR} retrieval techniques.

Acknowledgments. The authors thank the staff at the Chilbolton Facility of Atmospheric and Radio Research for their operation and maintenance of CAMRa, and Chris Walden in particular for his help with time series data acquisition. The first author was funded by a National Environmental Research Council Studentship.

APPENDIX

The Effect of Imperfectly Collocated *H* and *V* Samples on ρ_{hv}

Consider two measurements of the (complex) amplitudes at horizontal and vertical polarizations A_H and A_V. If the two polarizations do not have perfectly matched sample volumes, then each amplitude is the sum of (i) a component that is common to both polarizations C_H and C_V and (ii) a component that is different for each polarization D_H and D_V:

$$A_H = C_H + D_H \tag{A1}$$

(and similarly $A_V = C_V + D_V$). The copolar correlation coefficient is

$$\rho_{hv} = \frac{\sum A_H A_V^*}{\sqrt{\sum |A_H|^2 \sum |A_V|^2}}, \tag{A2}$$

where the sums Σ are taken over many reshufflings of the raindrops. Substituting in the expressions for A_H and A_V leads to

$$\rho_{\rm hv} = \frac{\sum C_H C_V^* + \sum D_H C_V^* + \sum C_H D_V^* + \sum D_H D_V^*}{\sqrt{\sum |C_H + D_H|^2 \sum |C_V + D_V|^2}}. \quad \text{(A3)}$$

The first term in the numerator dominates as the number of pulses is increased. This is because D_H and D_V are uncorrelated with C_V and C_H (because the reshuffling of particles in the different sample volumes is not connected or organized in any way) whereas C_H and C_V are highly correlated (because the true $\rho_{\rm hv}$ is close to 1). The final term is small because D_H and D_V are not correlated (by the same argument), and this term is small in any case since $|D| \ll |C|$.

This leaves the following:

$$\rho_{\rm hv} = \frac{\sum C_H C_V^*}{\sqrt{\sum |C_H + D_H|^2 \sum |C_V + D_V|^2}}. \quad \text{(A4)}$$

In the case of a perfect radar with perfect collocation of the H and V samples, then D_H and D_V are zero and we get a correlation coefficient that is the true $\rho_{\rm hv}$, which we are trying to obtain [i.e., setting $A = C$ in Eq. (A2)].

In general, for an imperfect radar, we have D_H and $D_V > 0$ and from the results above we see that

$$\rho_{\rm hv} = \rho_{\rm hv}^{\rm true} \times f_{\rm hv}^{\rm max}, \quad \text{(A5)}$$

where

$$f_{\rm hv}^{\rm max} = \left(\frac{\sum |C_H|^2}{\sum |C_H + D_H|^2} \times \frac{\sum |C_V|^2}{\sum |C_V + D_V|^2} \right)^{1/2}. \quad \text{(A6)}$$

This result is directly analogous to the results of Bringi et al. (1983) on $\rho_{\rm hv}$ in the presence of noise. If we identify C as our "signal" and D as our "noise," this equation is identical to Eq. (A1).

Crucially, the relationship between the true $\rho_{\rm hv}$ ($\rho_{\rm hv}^{\rm true}$) and the one that is actually observed is determined simply by how much power (on average over many pulses) comes from the particles that are different for the H and V sample volumes, relative to how much power comes from the particles that are common to the H and V sample volumes, and that this factor should be constant for different microphysical situations. Thus, if we can measure $\rho_{\rm hv}$ in drizzle where we know $\rho_{\rm hv}^{\rm true} = 1$, then the measured $\rho_{\rm hv}$ is simply equal to $f_{\rm hv}^{\rm max}$. This scaling factor can then be applied to data from all other situations.

REFERENCES

Andrić, J., M. R. Kumjian, D. S. Zrnić, J. M. Straka, and V. M. Melnikov, 2013: Polarimetric signatures above the melting layer in winter storms: An observational and modeling study. *J. Appl. Meteor. Climatol.*, **52**, 682–700, doi:10.1175/JAMC-D-12-028.1.

Balakrishnan, N., and D. Zrnić, 1990: Use of polarization to characterize precipitation and discriminate large hail. *J. Atmos. Sci.*, **47**, 1525–1540, doi:10.1175/1520-0469(1990)047<1525:UOPTCP>2.0.CO;2.

Beard, K. V., and R. J. Kubesh, 1991: Laboratory measurements of small raindrop distortion. Part 2: Oscillation frequencies and modes. *J. Atmos. Sci.*, **48**, 2245–2264, doi:10.1175/1520-0469(1991)048<2245:LMOSRD>2.0.CO;2.

——, V. Bringi, and M. Thurai, 2010: A new understanding of raindrop shape. *Atmos. Res.*, **97**, 396–415, doi:10.1016/j.atmosres.2010.02.001.

Brandes, E. A., and K. Ikeda, 2004: Freezing-level estimation with polarimetric radar. *J. Appl. Meteor.*, **43**, 1541–1553, doi:10.1175/JAM2155.1.

——, G. Zhang, and J. Vivekanandan, 2002: Experiments in rainfall estimation with a polarimetric radar in a subtropical environment. *J. Appl. Meteor.*, **41**, 674–685, doi:10.1175/1520-0450(2002)041<0674:EIREWA>2.0.CO;2.

Bringi, V. N., and V. Chandrasekar, 2001: *Polarimetric Doppler Weather Radar: Principles and Applications*. Cambridge University Press, 636 pp.

——, T. A. Seliga, and S. M. Cherry, 1983: Statistical properties of the dual-polarization differential reflectivity ($Z_{\rm DR}$) radar signal. *IEEE Trans. Geosci. Remote Sens.*, **GE-21**, 215–220, doi:10.1109/TGRS.1983.350491.

Cao, Q., and G. Zhang, 2009: Errors in estimating raindrop size distribution parameters employing disdrometer and simulated raindrop spectra. *J. Appl. Meteor. Climatol.*, **48**, 406–425, doi:10.1175/2008JAMC2026.1.

——, ——, E. Brandes, T. Schuur, A. Ryzhkov, and K. Ikeda, 2008: Analysis of video disdrometer and polarimetric radar data to characterize rain microphysics in Oklahoma. *J. Appl. Meteor. Climatol.*, **47**, 2238–2255, doi:10.1175/2008JAMC1732.1.

Caylor, I. J., 1989: Radar observations of maritime clouds using dual linear polarisation. Ph.D. thesis, University of Manchester Institute of Science and Technology, Manchester, United Kingdom, 261 pp.

——, and A. J. Illingworth, 1989: Identification of the bright band and hydrometeors using co-polar dual polarization radar. Preprints, *24th Conf. on Radar Meteorology*, Tallahassee, FL, Amer. Meteor. Soc., 352–357.

Doviak, R. J., and D. Zrnić, 2006: *Doppler Radar and Weather Observations*. 2nd ed. Dover Publications, 562 pp.

Fisher, R. A., 1915: Frequency distribution of the values of the correlation coefficient in samples from an indefinitely large population. *Biometrika*, **10**, 507–521.

Giangrande, S. E., J. M. Krause, and A. V. Ryzhkov, 2008: Automatic designation of the melting layer with a polarimetric prototype of the WSR-88D radar. *J. Appl. Meteor. Climatol.*, **47**, 1354–1364, doi:10.1175/2007JAMC1634.1.

Goddard, J., J. D. Eastment, and M. Thurai, 1994: The Chilbolton Advanced Meteorological Radar: A tool for multidisciplinary atmospheric research. *Electron. Commun. Eng. J.*, **6** (2), 77–86, doi:10.1049/ecej:19940205.

Illingworth, A. J., and I. J. Caylor, 1991: Co-polar correlation measurements of precipitation. Preprints, *25th Int. Conf. on Radar Meteorology*, Paris, France, Amer. Meteor. Soc., 650–653.

Jameson, A., 1987: Relations among linear and circular polarization parameters measured in canted hydrometeors. *J. Atmos. Oceanic*

Technol., **4**, 634–646, doi:10.1175/1520-0426(1987)004<0634:RALACP>2.0.CO;2.

——, and A. Kostinski, 1998: Fluctuation properties of precipitation. Part II: Reconsideration of the meaning and measurement of raindrop size distributions. *J. Atmos. Sci.*, **55**, 283–294, doi:10.1175/1520-0469(1998)055<0283:FPOPPI>2.0.CO;2.

Johnson, R. W., D. V. Kliche, and P. L. Smith, 2014: Maximum likelihood estimation of gamma parameters for coarsely binned and truncated raindrop size data. *Quart. J. Roy. Meteor. Soc.*, **140**, 1245–1256, doi:10.1002/qj.2209.

Liu, L., V. N. Bringi, V. Chandrasekar, E. A. Mueller, and A. Mudukutore, 1994: Analysis of the copolar correlation coefficient between horizontal and vertical polarizations. *J. Atmos. Oceanic Technol.*, **11**, 950–963, doi:10.1175/1520-0426(1994)011<0950:AOTCCC>2.0.CO;2.

McFarquhar, G. M., 2004: The effect of raindrop clustering on collision-induced break-up of raindrops. *Quart. J. Roy. Meteor. Soc.*, **130**, 2169–2190, doi:10.1256/qj.03.98.

Papoulis, A., 1965: *Probability, Random Variables, and Stochastic Processes*. McGraw-Hill, 583 pp.

Park, H. S., A. V. Ryzhkov, D. Zrnić, and K.-E. Kim, 2009: The hydrometeor classification algorithm for the polarimetric WSR-88D: Description and application to an MCS. *Wea. Forecasting*, **24**, 730–748, doi:10.1175/2008WAF2222205.1.

Rogers, R., 1989: Raindrop collision rates. *J. Atmos. Sci.*, **46**, 2469–2472, doi:10.1175/1520-0469(1989)046<2469:RCR>2.0.CO;2.

Sachidananda, M., and D. Zrnić, 1989: Efficient processing of alternately polarized radar signals. *J. Atmos. Oceanic Technol.*, **6**, 173–181, doi:10.1175/1520-0426(1989)006<0173:EPOAPR>2.0.CO;2.

Schafer, R., S. Avery, P. May, D. Rajopadhyaya, and C. Williams, 2002: Estimation of rainfall drop size distributions from dual-frequency wind profiler spectra using deconvolution and a nonlinear least squares fitting technique. *J. Atmos. Oceanic Technol.*, **19**, 864–874, doi:10.1175/1520-0426(2002)019<0864:EORDSD>2.0.CO;2.

Seliga, T., and V. Bringi, 1976: Potential use of radar differential reflectivity measurements at orthogonal polarizations for measuring precipitation. *J. Appl. Meteor.*, **15**, 69–76, doi:10.1175/1520-0450(1976)015<0069:PUORDR>2.0.CO;2.

Szakáll, M., K. Diehl, S. K. Mitra, and S. Borrmann, 2008: A wind tunnel study on the oscillation of freely falling raindrops. *Proc. Fifth European Conf. on Radar in Meteorology and Hydrology (ERAD 2008)*, Helsinki, Finland, Finnish Meteorological Institute, paper 7.6.

——, S. K. Mitra, K. Diehl, and S. Borrmann, 2010: Shapes and oscillations of falling raindrops—A review. *Atmos. Res.*, **97**, 416–425, doi:10.1016/j.atmosres.2010.03.024.

——, S. Kessler, K. Diehl, S. K. Mitra, and S. Borrmann, 2014: A wind tunnel study of the effects of collision processes on the shape and oscillation for moderate-size raindrops. *Atmos. Res.*, **142**, 67–78, doi:10.1016/j.atmosres.2013.09.005.

Tabary, P., A. Le Henaff, G. Vulpiani, J. Parent-du Châtelet, and J. Gourley, 2006: Melting layer characterization and identification with a C-band dual-polarization radar: A long-term analysis. *Proc. Fourth European Radar Conf. on Radar in Meteorology and Hydrology*, Barcelona, Spain, Centre de Recerca Aplicada en Hidrometeorologia, 17–20.

Tang, L., J. Zhang, C. Langston, J. Krause, K. Howard, and V. Lakshmanan, 2014: A physically based precipitation–nonprecipitation radar echo classifier using polarimetric and environmental data in a real-time national system. *Wea. Forecasting*, **29**, 1106–1119, doi:10.1175/WAF-D-13-00072.1.

Thurai, M., and V. Bringi, 2005: Drop axis ratios from a 2D video disdrometer. *J. Atmos. Oceanic Technol.*, **22**, 966–978, doi:10.1175/JTECH1767.1.

——, D. Hudak, and V. Bringi, 2008: On the possible use of copolar correlation coefficient for improving the drop size distribution estimates at C band. *J. Atmos. Oceanic Technol.*, **25**, 1873–1880, doi:10.1175/2008JTECHA1077.1.

——, M. Szakáll, V. N. Bringi, and S. K. Mitra, 2013: Collision-induced drop oscillations from wind-tunnel experiments. *Proc. 36th Conf. on Radar Meteorology*, Breckenridge, CO, Amer. Meteor. Soc., 9B.2. [Available online at https://ams.confex.com/ams/36Radar/webprogram/Paper228158.html.]

Tokay, A., A. Kruger, and W. F. Krajewski, 2001: Comparison of drop size distribution measurements by impact and optical disdrometers. *J. Appl. Meteor.*, **40**, 2083–2097, doi:10.1175/1520-0450(2001)040<2083:CODSDM>2.0.CO;2.

Torlaschi, E., and Y. Gingras, 2003: Standard deviation of the copolar correlation coefficient for simultaneous transmission and reception of vertical and horizontal polarized weather radar signals. *J. Atmos. Oceanic Technol.*, **20**, 760–766, doi:10.1175/1520-0426(2003)20<760:SDOTCC>2.0.CO;2.

Ulbrich, C. W., 1983: Natural variations in the analytical form of the raindrop size distribution. *J. Climate Appl. Meteor.*, **22**, 1764–1775, doi:10.1175/1520-0450(1983)022<1764:NVITAF>2.0.CO;2.

Unal, C., 2015: High resolution raindrop size distribution retrieval based on the Doppler spectrum in the case of slant profiling radar. *J. Atmos. Oceanic Technol.*, **32**, 1191–1208, doi:10.1175/JTECH-D-13-00225.1.

Williams, C. R., 2002: Simultaneous ambient air motion and raindrop size distributions retrieved from UHF vertical incident profiler observations. *Radio Sci.*, **37**, doi:10.1029/2000RS002603.

——, and Coauthors, 2014: Describing the shape of raindrop size distributions using uncorrelated raindrop mass spectrum parameters. *J. Appl. Meteor. Climatol.*, **53**, 1282–1296, doi:10.1175/JAMC-D-13-076.1.

Wilson, D. R., A. J. Illingworth, and T. M. Blackman, 1997: Differential Doppler velocity: A radar parameter for characterizing hydrometeor size distributions. *J. Appl. Meteor.*, **36**, 649–663, doi:10.1175/1520-0450-36.6.649.